Nuclear Magnetic Resonance Spectroscopy of Hydrated Carbon Based Materials

A thesis submitted in partial fulfillment of the requirements for the degree of Bachelor of Science in Physics from the College of William and Mary in Virginia.

Advisors: Gina L. Hoatson and Robert L. Vold

By: Rebekah L. Blount

Williamsburg, VA
May 5, 2005

The heavens declare the glory of God;
the skies proclaim the work of his hands.
Day after day they pour forth speech;
night after night they display knowledge.
May the words of my mouth and the meditation of my heart
be pleasing in your sight,
O Lord, my Rock and my Redeemer.

Psalms 19:1-2, 14

Table of Contents

Acknowledgements

This thesis is dedicated to my parents, Micky and Sandy Mitchell who made a lot of sacrifices to put me through school and helped me stay at William and Mary so that I could finish my degree. Without them, I could never have come so far.

I'd also like to thank my professors, Gina Hoatson and Robert Vold for all the time they put into teaching me the science of NMR and helping me coordinate my thoughts to bring this paper about.

Last, but not least, I'd like to thank Yuanyuan Huang for all of the countless hours he spent helping me run my experiments and learning to run the spectrometer. I know I'll never be able to repay him for his kindness, time, and patience in teaching me.

List of Figures

List of Tables

Abstract

Carbon nitride films (α-CN_x) have the unusual combination of two properties, hardness and elasticity which suggest a variety of important applications. When hydrated these properties deteriorate. By studying hydrated graphite samples and other carbon based materials, we hope to further understand the water adsorption properties. Using Nuclear Magnetic Resonance spectroscopy (NMR) we hope to determine how much water is adsorbed on the film and the nature of the absorption sites.

Chapter 1

Introduction

1.1 Carbon Nitride Films (α-CN_x)

Carbon nitride films (α-CN_x) are thin layers deposited with atomic ratios of approximately 80% carbon (^{12}C) and 20% nitrogen (^{14}N). They are prepared by vacuum deposition on a substrate such as a silicon wafer. Amorphous carbon materials are primarily used as protective coatings for hard disk drives and have the unique property of being both hard and elastic simultaneously. Adding nitrogen to the carbon films retains this unique combination of desired properties and results in a reduction of the thickness of the film. From previous NMR experiments, it was found that heating the α-CN_x to approximately 150 ^{o}C caused a two fold decrease in the intensity of the broad, asymmetric line in the proton NMR spectrum [1]. These results suggest that water is binding to the material. From NMR measurements, the researchers hypothesized that the water is preferentially bonded to the nitrogen sites of the film, possibly by a hydrogen bond. However, the degree to which the water penetrates into the bulk material remains unknown [1,2].

In my experiments, I will explore the extent to which the water is adsorbed on the thin films of α-CN_x. To investigate this hypothesis, we are going to record and interpret

^1H and ^2H NMR spectra from carbon based films exposed to controlled percentage humidity chambers containing both H_2O and D_2O. From these spectra, we will be able to detect the presence of hydrogen bonds and the amount of ^1H_2O and ^2H_2O that has been adsorbed. Interpretation of the adsorption sites is more easily done with ^2H NMR than ^1H NMR because the deuteron has a nuclear quadrupole moment which couples with the local electric field gradients. This interaction eases the spectral interpretation because the peaks are usually better resolved than in the ^1H spectrum.

1.2 Graphite

The α-CN_x thin films are very expensive and time consuming to make, especially the amount needed for NMR experiments. Therefore, to initiate the study of water adsorption, I will investigate the adsorption on graphite, a carbon based compound that has a similar molecular structure to the carbon nitride films. The structure of graphite (as seen in Fig. 1.1) consists of hexagonal carbon rings connected to each other through sp^2 hybridized covalent bonds. These sheets of rings then stack on top of each other and are bonded together through weak Van der Waals forces. Because these weak forces hold the sheets together, the graphite layers are able to slide over each other, giving graphite its lubricating properties. In each sheet, the delocalized pi electron is free to move throughout the carbon atoms pi orbitals within its perspective sheet. This causes the bonds between the carbon atoms to be very strong because these free electrons form

alternating double bonds between the molecules giving the graphite rings a structure similar to benzene [3,4].

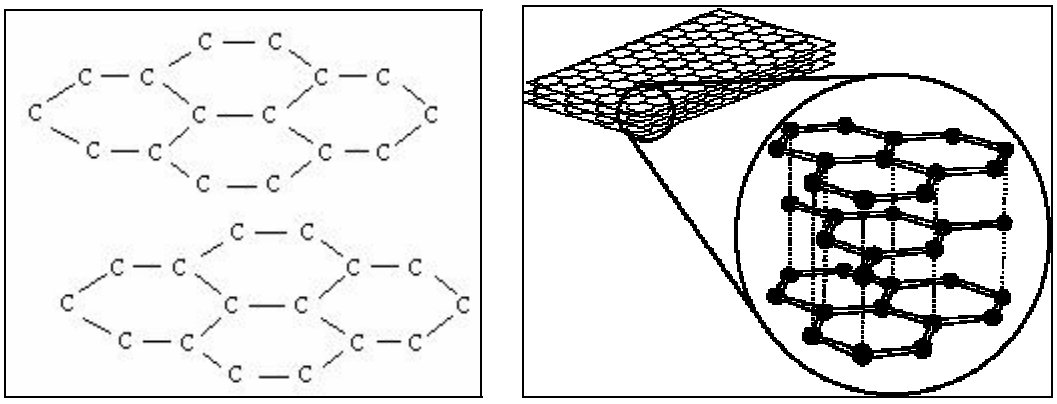

Figure 1.1: The picture on the left is a picture of the molecular diagram of graphite which shows the sp^2 hybridization and the bonding of the carbon molecules to each other [3]. The picture on the right shows the sheets of graphite. The dotted lines are the Van der Waals forces that bond the graphite sheets and allow the layers to slip and slide over each other [4].

Comparing the structure of the α-CN_x to the structure of graphite, we can see many similarities. The carbon atoms are arranged in hexagonal rings and have sp^2 hybridization. The nitrogen atoms are incorporated into the carbon rings by substituting for the carbon or bonding to the carbon on the edges of the ring; this bond is also sp^2 hybridized. The similarities of the structures can be seen by comparing the graphite structure in Fig. 1.1 with the α-CN_x structure in Fig. 1.2 [5].

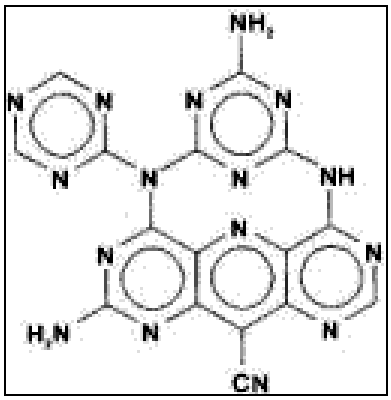

Figure 1.2: The structure of amorphous α-CN_x films. From the structure the similarities to graphite can be seen [5].

1.3 Carbon Nanoflakes

A second carbon based compound that we experiment with is carbon nanoflakes. Carbon nanoflakes are a newly developed material. The nanoflakes are made using heat deposition onto a substrate such as silicon. Much research is being done on the nanoflakes to determine their structure. What is known about them is that they are quasi two dimensional nanoscale sheets of carbon less than 10 nm in thickness. Once deposited the nanoflakes stand vertically upon the substrate. This increases the surface area of adsorption on the films which makes them a good material for our study [6,7].

1.4 Carbon Nanotubes

A final material of interest that we didn't experiment on but would be necessary to test with in future experiments are carbon nanotubes. Nanotubes also have a similar structure to graphite. As seen in Fig. 1.3, a carbon nanotube is simply a sheet of nanosized graphite, rolled into a tube, and bonded to itself creating the strongest fibers on

earth that are currently known. The hybridization remains sp^2 which maintains the delocalized electrons that are free to roam throughout the nanotube, governed by the laws of quantum mechanics. This delocalization allows the nanotube to take on a variety of electric properties. Depending on how the nanotube is folded, it can be a semiconductor or a metal or both within the same nanotube [8].

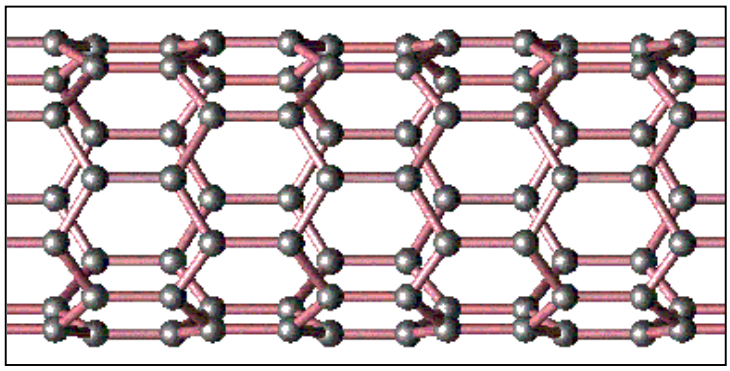

Figure 1.3: The structure of a carbon nanotube [8].

Chapter 2

Theory

2.1 NMR Spectroscopy

NMR spectroscopy is based in the concepts of quantum mechanics particularly the concept of spin. Some nuclei have spin, or angular momentum, which in turn creates a magnetic moment (μ) given by the following equation:

$$\mu = \gamma I \hbar, \qquad (1)$$

where γ is the magnetogyric ratio, $\hbar$ is Planck's constant over 2π, and I is the nuclear spin quantum number. For any nucleus with angular momentum quantum number I, there are $(2I + 1)$ possible spin component values, I_z. These correspond to discrete spin states. In the absence of a magnetic field, all spin states have the same energy. However, when placed in a static magnetic field (B_0), the Zeeman interaction shifts these energy levels and the quantized, allowable energies are given by the following equation:

$$E_j = -\hbar\gamma I_z B_0 \qquad (2)$$

in which I_z is the magnetic component quantum number. NMR spectroscopy capitalizes on these energy differences of spin states [9].

When placed into a magnetic field, the nuclei begin to precess about the magnetic field. In NMR a static magnetic field (B_o) defines a the z-axis and causes the nucleus to begin to precess around the magnetic field at a certain frequency called the Larmor frequency (υ_0), as seen in Fig. 2.1. This frequency is nucleus specific and can be defined mathematically as:

$$\upsilon_0 = \gamma B_0/2\pi. \qquad (3)$$

The net magnetization is defined by

$$M = N_l - N_{u,} \qquad (4)$$

where N_u is the number of spins in the higher energy level and N_l is the number of spins in the lower energy level.

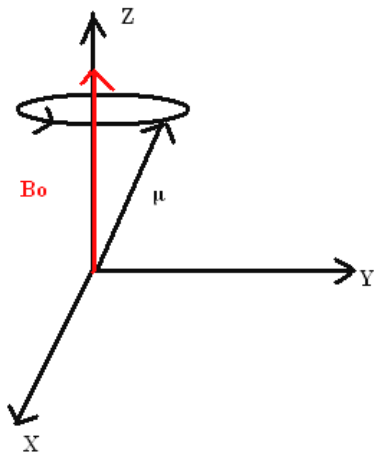

Figure 2.1: A nucleus with magnetic moment μ precessing about a static magnetic field B_0 along the z-axis.

When a time dependent radiofrequency is pulsed in a coil perpendicular to the magnetic field at the same "resonance" frequency as υ_0, the spin of the nucleus will "flip" from a lower energy level to a higher energy level resulting in absorption of energy. When the nucleus spin flips, a voltage is induced in the sample coil; this free induction decay (FID) signal is what is measured in an NMR experiment [10].

After the nucleus has been pulsed and the spin has jumped to a higher energy level, it must then return to its original lower energy state. The spin system has to "relax" back to thermal equilibrium, this occurs in a time known as longitudinal spin relaxation time, T_1. In addition, as the spin begins to precess in the xy plane, dephasing and transverse relaxation, T_2, cause the inducted voltage in the coils to decay in time. This time domain signal is digitized by ADC's in the receiver is known as free induction decay (FID). The time domain FID is Fourier transformed to give the NMR frequency spectrum [10].

For atoms which have a spin I = ½, experiments are relatively simple. For this spin, there are two quantized energy levels; the lower level being for $I_z = + ½$ and the higher level for $I_z = - ½$. This relationship is illustrated in Fig. 2.2. More nuclei are

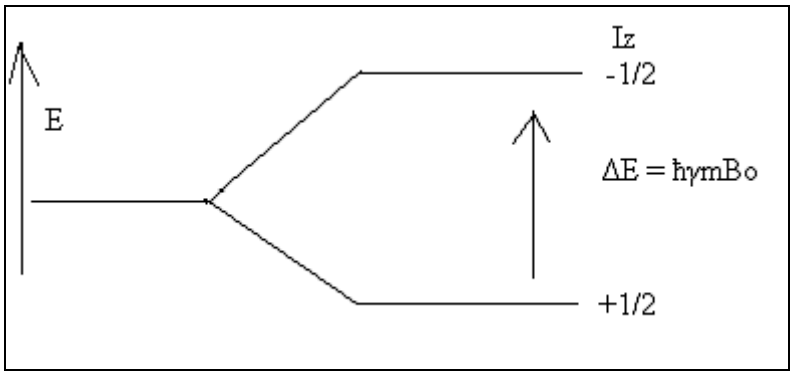

Figure 2.2: Diagram showing the energy levels of a nucleus with spin state I=1/2.

expected to reside in the lower energy level and their distribution is described by a Boltzmann distribution:

$$N_u/N_l = \exp(-\Delta E/kT) \qquad (4)$$

in which N_u is the number of nuclei in the upper energy level, N_l is the number of nuclei in the lower energy level, and k is the Boltzman constant. If the spin is greater than ½ then the description becomes more complex since other spin interactions begin to enter the picture [9]. The interaction of greatest importance to the experiments described in this thesis will be the quadrupolar interaction of the deuteron, I = 1. But before we get to the quadrupolar interaction, we must first discuss magic angle spinning.

2.2 Magic Angle Spinning

Magic angle spinning (MAS) is a technique used to help eliminate the anisotropic interactions in solids. For example, when two different nuclei are placed in a magnetic field a distance r away from each other, the dipolar field of the nuclei modifies the static magnetic field, B_0, and this affects the observed frequency of the second nuclei. Since B_0 is along the z axis, the change in the magnetic field is:

$$B_z = (\gamma_1\gamma_2\hbar\mu/r^3)(3\cos^2\theta - 1), \quad (5)$$

where θ is the angle between B_0 and the internuclear vector. The angle at which $(3\cos^2\theta - 1) = 0$ is 54.44^o and this angle is called the magic angle. When the rotor is oriented at this angle and then the sample is spun, all of the terms depending on $(3\cos^2\theta - 1)$ cancel. This eliminates all second rank tensor interactions including the heteronuclear dipolar coupling. This technique works well for spins with I=1/2 [9].

The deuteron (^{2}H) has a spin value I = 1. This spin quantum number results in quadrupolar interaction which is a result of the non-spherical, asymmetric charge distribution of the nucleus interacting with the local electric field gradients. The quadrupole interaction adds an additional term to the Hamiltonian and energy. Only one term in the Hamiltonian depends on $(3\cos^2\theta - 1)$, therefore using MAS on a quadrupolar nucleus, the second-order term is not completely eliminated by the magic angle spinning but it is greatly reduced. If there are any heteronuclear dipole-dipole affects, they will be eliminated by the MAS. Because of this observation, for deuterons it is preferable to complement ^{2}H MAS measurements with static quadrupole echo experiments to get optimal results.

2.3 Static Quadrupole Echo Experiment

The quadrupole echo experiment is a pulse technique used to help get undistorted better resolved spectra on spins experiencing dipolar or quadrupolar couplings. This experiment is comprised of two pulses; the pulse sequence can be seen in Fig. 2.3. The initial excitation pulse is a 90_x^O pulse along the x-axis and then there is a time of free evolution. Next a second, 90_y^O pulse applied along the y-axis. The FID is measured after this second pulse which refocuses the magnetization along this axis [11,12]. By refocusing the spins, a stronger signal is attained outside the electronic dead line of the probe.

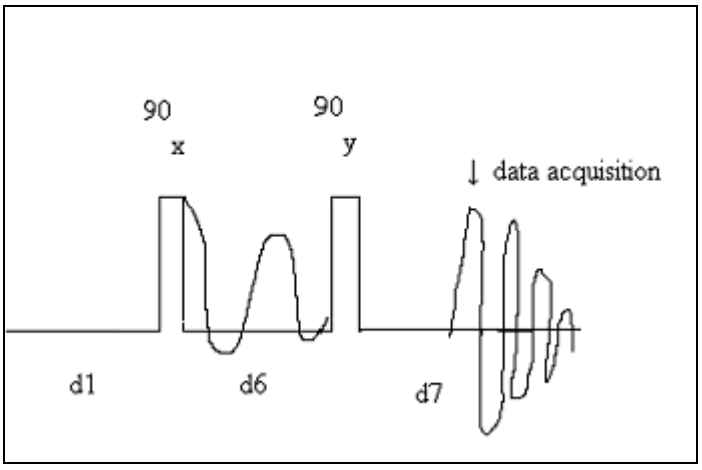

Figure 2.3: The pulse sequence of the quadrupole echo: 90_x^O pulse followed by a 90_y^O pulse. Acquisition of data is started before maximum height of the peak after the second pulse to receive the optimum signal.

2.4 Spinning Quadrupole Echo Experiment

The spinning quadrupole echo experiment combines the techniques of magic angle spinning and the quadrupole echo pulse sequence. This experiment is more complicated than the static QE experiment because it requires synchronization of the spinning rotor with the time between the two radiofrequency pulses. If this synchronizing isn't done, it can result in interference with the pulse and the rotary echo formation.

Chapter 3

Experimental Techniques

As a preliminary experiment, we investigated graphite samples because graphite is an abundant and cheap carbon based material and has many similarities to the carbon in the α-CN_x. We began with the graphite sample because of the small amount of α-CN_x samples available are very precious since they are time consuming to make. Beginning with graphite, we wanted to see if enough D_2O would adsorb onto the surface for us to obtain a detectable NMR signal. The calibration was done using liquid D_2O and salts to create chambers of known relative humidity. The range of humidities was from 11-97 percent at room temperature depending on the type of salt used [13, 14].

3.1 H_2O vs. D_2O

To begin the experiment, I created two chambers. One contained a saturated solution of potassium sulfate (25 ml of D_2O with an excess of K_2SO_4) to create a relative humidity of 97%. The second chamber was identical except H_2O was used instead of D_2O. Once the solutions were mixed, known amounts of graphite were placed on platforms in the solution and the chambers were closed with parafilm to maintain the constant, known humidity environment. The graphite sat in these chambers for several days in order to equilibrate and ensure as much D_2O and H_2O was adsorbed as possible. Upon taking the graphite out of the chambers, it was re-weighed and then packed into a rotor and run on the spectrometer.

With these two graphite samples, I was able to run several single pulse experiments. The experiments were run on a Bruker Advance spectrometer operating at 7T (^{1}H Larmor frequency of 300.07 MHz and ^{2}H Larmor frequency of 46.06 MHz). Each sample was packed into a 2.5 mm rotor and was irradiated with a 90_x^O pulse of length 2.1 μsec and attenuation level of 1.2 dB. The graphite samples hydrated with H_2O were investigated using proton NMR at 300 MHz. We did two different single pulse experiments, one static and another using magic angle spinning (MAS) at 25 kHz. The pulse sequence for the single pulse experiment can be seen in Fig. 3.1. The details of the typical number of scans and recycle delays (τ_d) are found in the Fig. 4.1 caption.

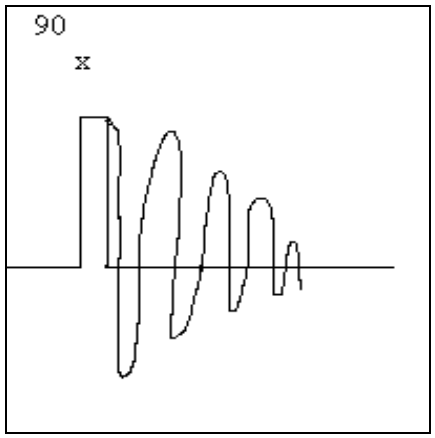

Figure 3.1: An illustration of the single pulse experiments.

The sample hydrated with D_2O was run using ^2H NMR on resonance at 46.06 MHz. On this sample, we irradiated the deuterons using a single 90_x^O pulse with MAS at 10 kHz. The details of the number of scans and τ_d is found in the Fig. 4.2 caption.

3.2 D_2O Hydrated Graphite Samples at Various Humidities

After running the initial experiments, I created three more chambers in addition to the 97% humidity chamber. Using D_2O and additional calibrating solutions, I was able to make a chamber with 85% relative humidity (excess of KCl), a chamber of 53% relative humidity (excess of $Mg(NO_3)_2$), and a chamber of 43% relative humidity (excess of K_2CO_3). Experiments were run on all four of these samples using a Bruker Advance spectrometer. Each sample was packed into a 2.5 mm rotor and we ran MAS experiments on these samples, along with a static quadrupole echo experiments. All

three of these experiments were on resonance. The single pulse MAS experiments were done with hard pulses with pulse length equal to 1.6 μsec at an attenuation level of 1.2 dB. The quadrupole echo experiments were done at an attenuation level of 3.10 dB, corresponding to a 90^{O} pulse length of 1.8 μsec. The recycle delay between the pulse sequences (d1) was set to 1 sec. The length of the first pulse along the x-axis (p1) was equal to the length of the second pulse (p2) along the y-axis which was set to 1.8 μsec. The delay between the two pulses (d6) was set to 30.2 μsec and the delay time between the second pulse and acquisition (d7) was set to22 μsec to ensure digitization of the echo maximum.

3.3 D_2O Hydrated Carbon Nanoflakess

After looking at the graphite samples, we decided to test a second carbon based material, carbon nanoflakes. To study adsorption on these, we wanted to compare the spectra we obtained from the graphite and see if the nanoflakes had similar characteristics and shapes to that of the graphite. This hydration was done in a slightly different manner than the graphite experiments.

The carbon nanoflakes that we obtained were deposited on two silicon wafers. In order to have the maximum surface area, we had to leave the nanoflakes on the wafer to adsorb the D_2O. We placed the wafers into sealed plastic bags, onto a platform. Then, we placed D_2O solution into the bags. To increase the rate of adsorption, we heated the bags for an hour with a hair dryer. This would speed up the creation of a humid environment. Once we noticed that sufficient D_2O was in the air and on the sides of the

bags, we turned off the hair dryer and let the samples sit in the humid environment overnight. After equilibration we scraped the nanoflakes off of the silicon substrate and loaded the rotor. On these samples, we performed a static, QE experiment using the same pulse parameters we used on the graphite with a pulse length equal to 1.6 μsec and an attenuation level of 3.10 dB. The recycle delay between the pulse sequences was 1sec, the length of both pulses was 1.8 μsec, the delay between the two pulses was 30.2 μsec and the delay to acquisition was 22 μsec.

Chapter 4

Results

4.1 H_2O vs. D_2O

From the graphite samples hydrated in the water solution, we were able to find that there was a significant amount of water adsorbed on the graphite. As seen in Fig. 4.1, the static signal has two peaks that have a width at half height of 14.7 kHz.

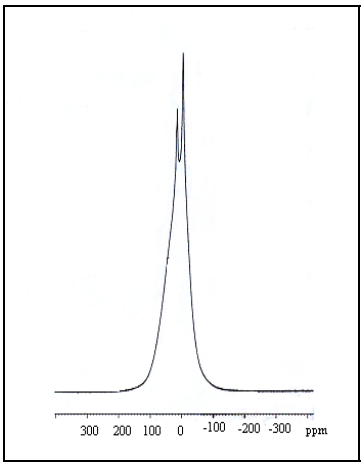

Figure 4.1: The sample that was run using ^{1}H NMR. It was a static, single 90_x^O pulse created in 64 scans with $\tau_d = 4.5$ μsec. The chemical shift of the first peak is 5586 Hz while the chemical shift of the second peak is 0 Hz. The width at half height is 14.7 kHz.

This line was quite broad so we performed a MAS experiment spinning at 25 kHz. The sample was irradiated with a single, 90_x^o pulse. This signal was obtained in 64 scans with a $\tau_d = 4.5$ μsec. The spinning of the sample caused the two peaks to separate and become individual peaks: chemical shift of the small peak is $\delta_1 = 5585$ Hz and the chemical shift of the second, larger peak is $\delta_2 = 739$ Hz. The width at half height of the second peak is 776 Hz. We think that the two peaks are due to the dipolar coupling interaction between the hydrogens in water.

In the samples hydrated with heavy water deuterons the results confirmed the proton results obtained using the H_2O hydrated samples. The first experiment we ran mimicked the experiment run on the proton hydrated samples. We ran a single, 90^O pulse experiment but obtained no noticeable signal. This was to be expected because the quadrupole moment of the ^{2}H nuclei makes the signal very small and difficult to detect. Since we didn't obtain a signal with the static single pulse experiment, we performed a single pulse MAS experiment.

These MAS experiments were run spinning at 10 kHz. From this technique, we were able to get a single peak with a width of 49 Hz, as seen in Fig. 4.2. These results show that deuterium has in fact adsorbed on the surface of the graphite. These results confirm the conclusions drawn from the study of the H_2O hydrated samples.

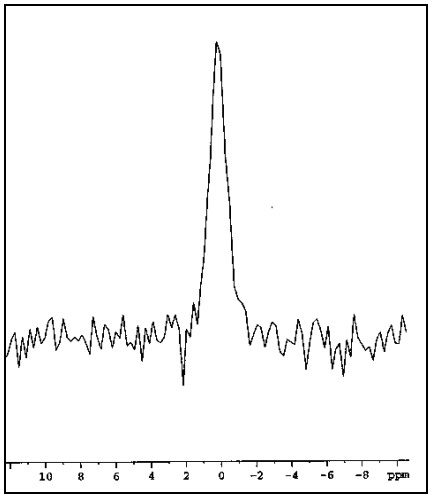

Figure 4.2: Graphite hydrated in a 97% D_2O solution. The experiment was performed using ^2H NMR with MAS at 10 kHz. The sample was irradiated with a single 90^o pulse and was obtained with 256 scans and $\tau_d = 8.93$ μsec. The chemical shift is 0.028 Hz and the width at half height was 49 Hz.

4.2 D_2O Hydrated Graphite Samples at Various Humidities

Using the graphite samples hydrated in the D_2O constant humidity chambers we ran several different NMR experiments. We began by running single pulse MAS

experiments on the four different hydrated samples followed by static quadrupole echo experiments. The results from these experiments are as follows.

We performed the MAS experiment spinning at 10 kHz on the samples hydrated in 97%, 85%, and 53% humidity solutions. The results were quantitatively similar to the results for the 97% hydrated sample discussed in the previous section. Results for the 85%, and 53% humidities are shown in Figs. 4.3 and 4.4 respectively. In all three of these experiments, the conditions remained identical and the only difference was the humidity percentage of the hydrating D_2O solution.

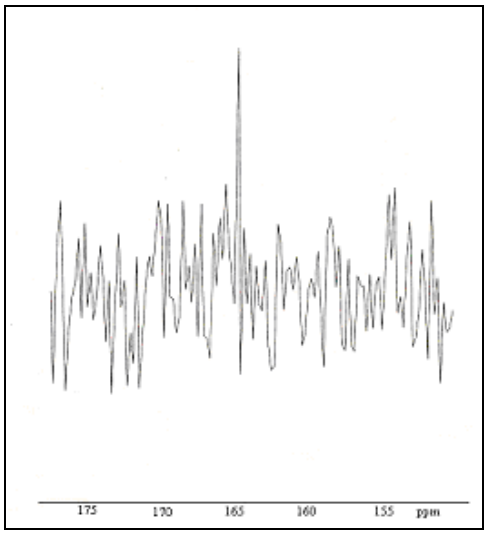

Figure 4.3: Graphite hydrated in an 85% D_2O solution using ^2H NMR with MAS at 10 kHz. The sample was irradiated with a single 90^o pulse and was obtained with 256 scans and τ_d = 8.93 μsec. The chemical shift is 7598 Hz and the width at half height was 19.5 Hz.

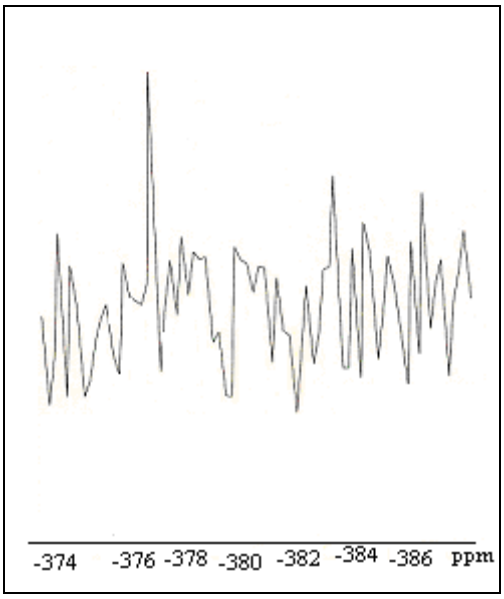

Figure 4.4: Graphite hydrated in a 53% D_2O solution using ^2H NMR with MAS at 10 kHz. The sample was irradiated with a single 90^o pulse and was obtained with 256 scans and τ_d = 8.93 μsec. The chemical shift was -17.6 Hz and the width at half height was around 10 Hz.

From each of these samples, the width of the spectral line decreases with decreasing humidity. These results are consistent with the hypothesis that less D_2O is adsorbed at lower percent humidity. A summary of the results of the varying humidity experiments done with deuteron magic angle spinning are summarized in Table 4.1.

Humidity Percent	δ (kHz)	Δ (kHz)
97%	0.028	49
85%	7.6	19.5
53%	-17.4	10

Table 4.1: A summary of the results of ^{2}H MAS experiments: δ = the chemical shift (Hz) and Δ = the width at half height (Hz).

In addition to the MAS experiments, we also ran static quadrupole echo experiments on all four of these samples. These experiments were run using the QE pulse sequence shown in Fig. 2.3, and all four samples had a τ_d = 4.5 μsec. When interpreting these spectra, we used DMfit simulation software [15]. We fit each spectrum to a simulated QE spectrum. We also used the simulation to calculate the δ shift of each peak (a combination of the chemical shift and the quadrupole shift), the amplitude of the peak, Lb factor (the exponential multiplication related to the dipolar coupling), nuQ (a symmetry factor related to line broadening), and etaQ (a curve symmetry factor).

Looking first at the sample hydrated in 97% humidity, we can see the convergence of the two peaks (see Fig. 4.3). This spectrum shows that the two separate peaks we'd expect to see from a QE experiment overlapped. We believe that this is due to the fact that so much D_2O has adsorbed onto the surface that it caused the signal to collapse. Further support of this hypothesis comes from research done on graphite water adsorption in which it was found that at humidities above 90%, there is the formation of

several water layers and "islands" of water that can form and that move around to create even larger regions. This shows that at these high humidities, large quantities of water build up on the surface of the thin films. [16]

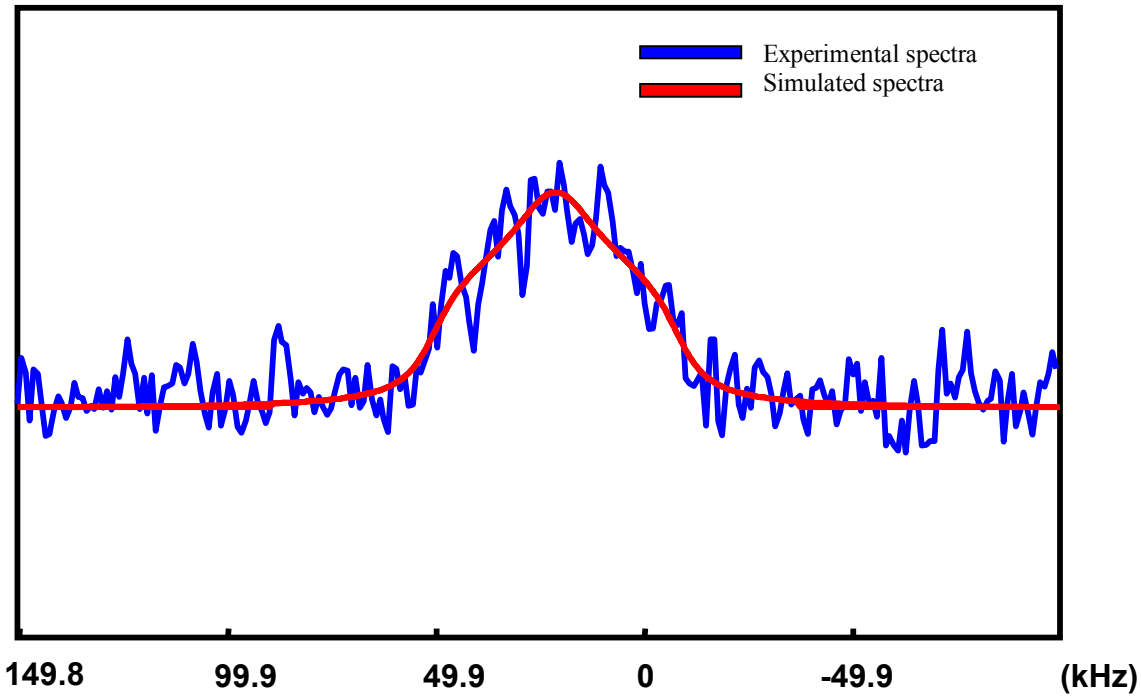

Figure 4.5: Graphite hydrated in 97% D_2O solution, using a static QE experiment with d1 = 1 sec, d6 = 30 μsec, and d7 = 22 μsec. This spectrum was taken in 40, 960 scans with 2048 data points.

Looking at the sample hydrated with D_2O in an 85% relative humidity, the two distinct peaks of the quadrupole echo are visible (see Fig. 4.6). From the presence of these peaks, we are able to see that D_2O has in fact adsorbed onto the surface at this humidity. Looking at the spectrum obtained at 85% humidity, the right edge of the spectrum seems to be cut off. We believe that this is actually the formation of the other side of the quadrupole peak that has been averaged. The peak that appears in the center of the spectrum, with a chemical shift of zero, is very pronounced and looks like some

pure liquid D2O in the sample that was either sitting on top of the surface, unabsorbed, or released from the sample due to time spent in the rotor.

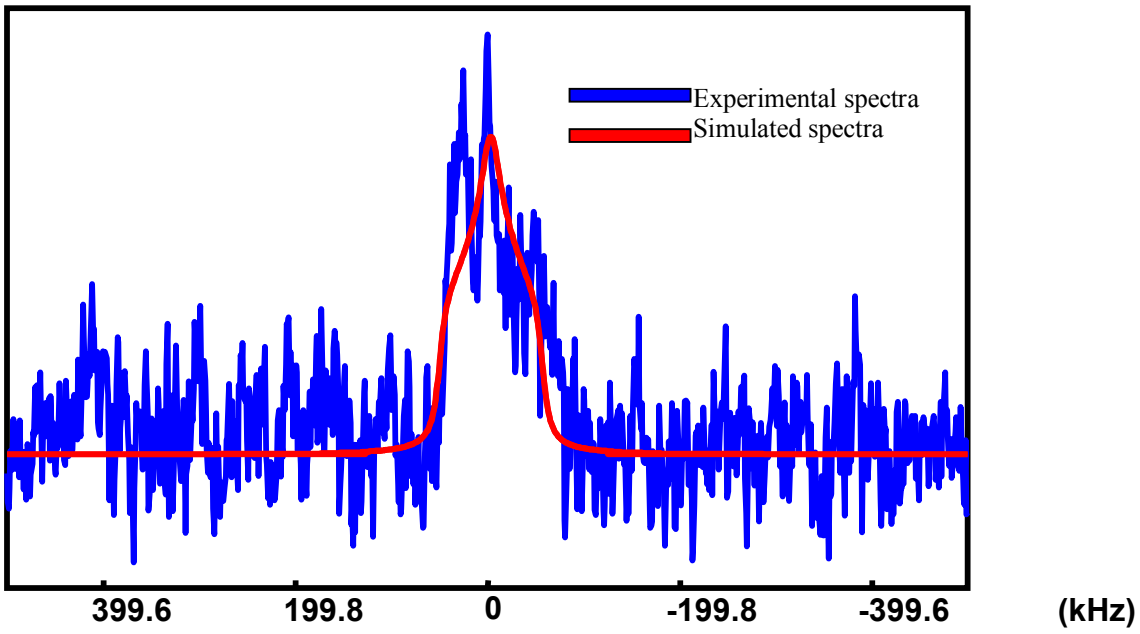

Figure 4.6: Graphite hydrated with D_2O in an 85% relative humidity solution using a static QE experiment with d1 = 1.0 sec, d6 = 30 µsec, and d7 = 22 µsec. The spectrum was taken with 4,000 scans and 2,048 data points.

The sample hydrated in the 53% relative humidity also had similar spectral peaks to the previous samples however the peak decreased in intensity and became much noisier due to the decreasing humidity. This suggests that as the relative humidity decreases, the amount of water adsorbed on the graphite decreases. The results for the graphite hydrated in 53% humidity can be seen in Fig. 4.7.

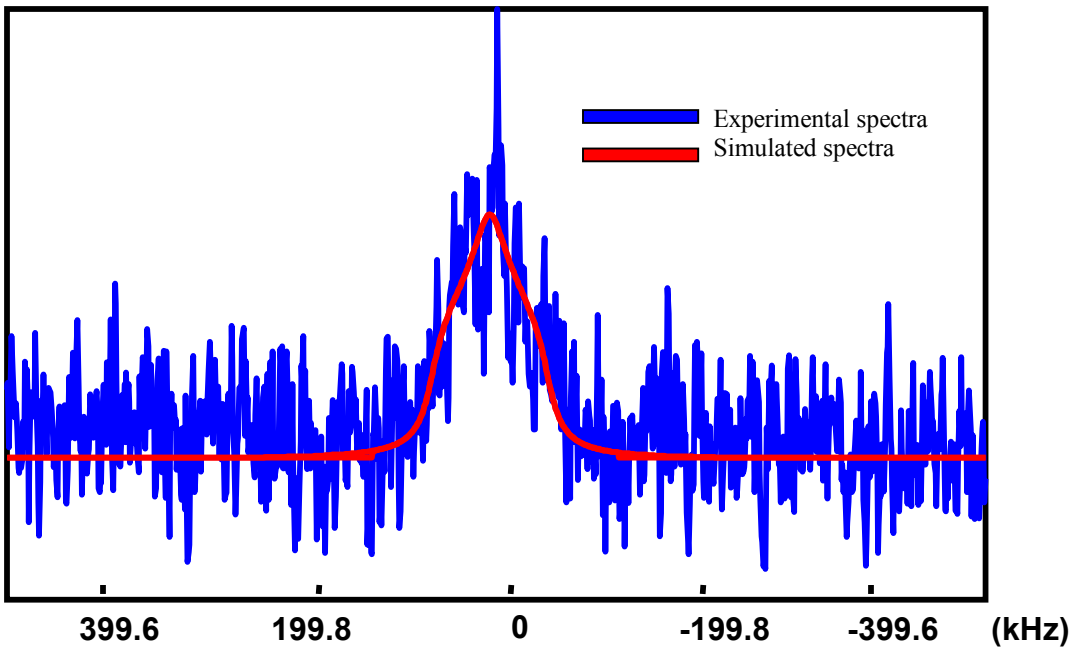

Figure 4.7: Graphite hydrated with D_2O in a 53% relative humidity solution using a static QE experiment with d1 = 1.0 sec, d6 = 30 µsec, and d7 = 22 µsec. The spectrum was taken in 2,048 scans with 2,048 data points.

The results for the graphite hydrated in 43% humidity were also similar to the three previous peaks. Like the other spectra, this sample continued the trend of decreased intensity and larger signal to noise that we believe is due to the smaller amount of D2O present in the sample. The 43% spectrum is similar to the 85% spectrum (seen in Fig. 4.6) in that the right side of the spectrum is clipped. Like the 85% spectrum, we believe that this clipping is due to the creation of a quadrupole peak with the pure D2O peak in the center. These two different sites cause signal averaging which causes the distortion seen in the spectrum. Also, the simulation fit is also not as good in this spectrum as it is in the others. This is due to the large amount of noise in the sample and the fact that there was so little D_2O in the sample that measurement of this D_2O is more difficult. The results for the sample hydrated at 43% relative humidity is seen in Fig. 4.8.

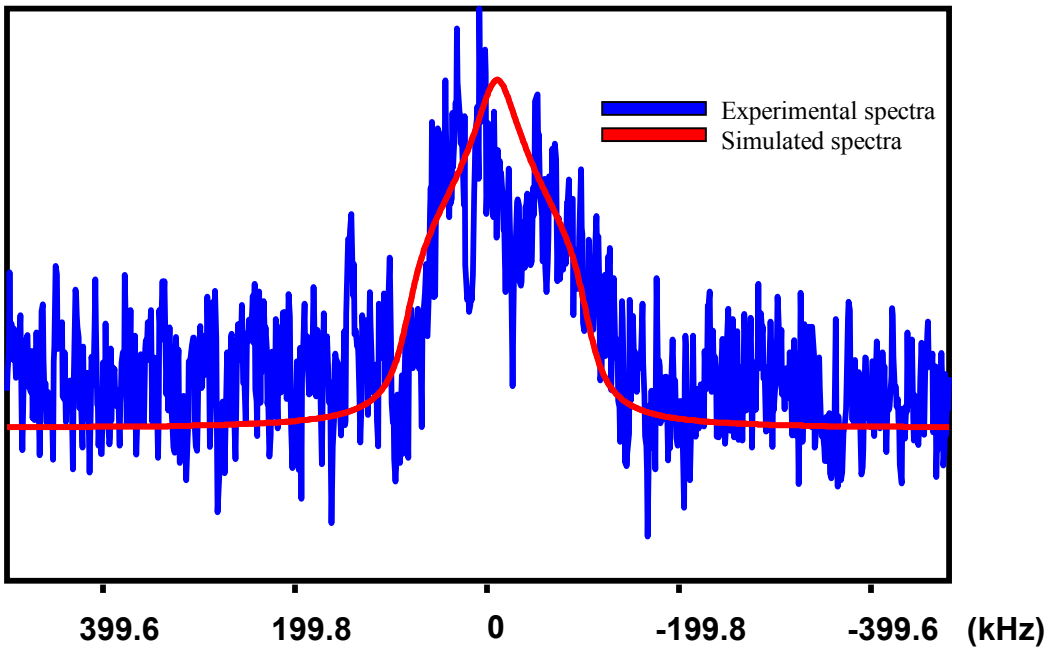

Figure 4.8: Graphite hydrated with D_2O in a 43% relative humidity solution using a static QE experiment with d1 = 1.0 sec, d6 = 30 µsec, and d7 = 22 µsec. The spectrum was taken with 2,048 scans and 2,048 data points.

A summary of the data for the static QE experiments can be found in table 4.2. In this table, it is easy to compare the four experiments. Fig. 4.9 shows a plot of nuQ versus percent humidity. From the graph, it is clearly shown that as the percent humidity increases the signal broadening decreases and the spectrum doesn't cover as wide a range of kHz. Also, from the nuQ we can determine that as the nuQ decreases, amplitude increases, and molecular motion becomes faster. This indicates that as the percent humidity increases, there is more D_2O on the sample.

Humidity Percent	δ (kHz)	Amp	LbHz(kHz)	nuQ(kHz)	etaQ
97%	21.4	6.80	11.1	61.13	0.84
85%	-3.4	1.77	11.0	110.0	0.90
53%	6.8	1.00	23.9	118.3	0.99
43%	-20.0	1.41	33.9	190.0	0.99

Table 4.2: A summary of the ^{2}H static QE experiments. δ = the position function that takes into account the chemical shift and the quadrupole shift. Amp = the relative height of the peak. LbHz = the exponential multiplication related to the dipolar coupling. nuQ = factor that takes into account both motion and amplitude of the peak, and etaQ = the relative symmetry of the curve.

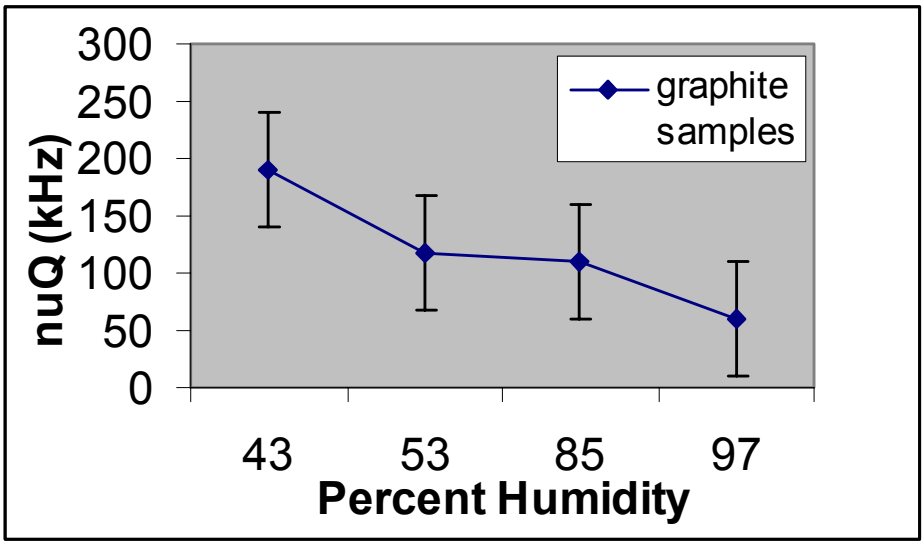

Figure 4.9: Graph of the nuQ versus the percent humidity of static QE experiments run on the graphite samples hydrated with D_2O solutions.

4.3 D_2O Hydrated Carbon Nanoflakes

The results for the carbon nanoflakes hydrated with D_2O were very similar to the results of the graphite samples. As can be seen in Fig. 4.10, the spectrum has the two spikes that we expect to see from a quadrupole echo sequence. Using the DM fit simulation sequence we were able to fit a simulated curve. The results from the simulation show that the actual spectrum is much more closely matched than it was in the graphite samples. Also, we were able to change the recycle delay time and confirmed that the dip between the two peaks is resulting from the quadrupole interactions and not due to the recycle delay time being too short. The results for the simulation are summarized in table 4.3. Also in the table are the data from the QE experiment on graphite at 85%. While we don't know the exact percent humidity in the bags, we can expect that it was large due to the heating of the environment and the visibility of D_2O along the sides of the bag. Comparing the shapes of the two spectra, the nanoflakes most closely resemble the 85% hydrated graphite sample because both samples have distinctive spikes on either side of the spectra resembling the QE line shape. Also, comparing the numbers, both curves have similar nuQ values. From these values and spectra, we can see that the nanoflakes and the graphite have similar water adsorption patterns.

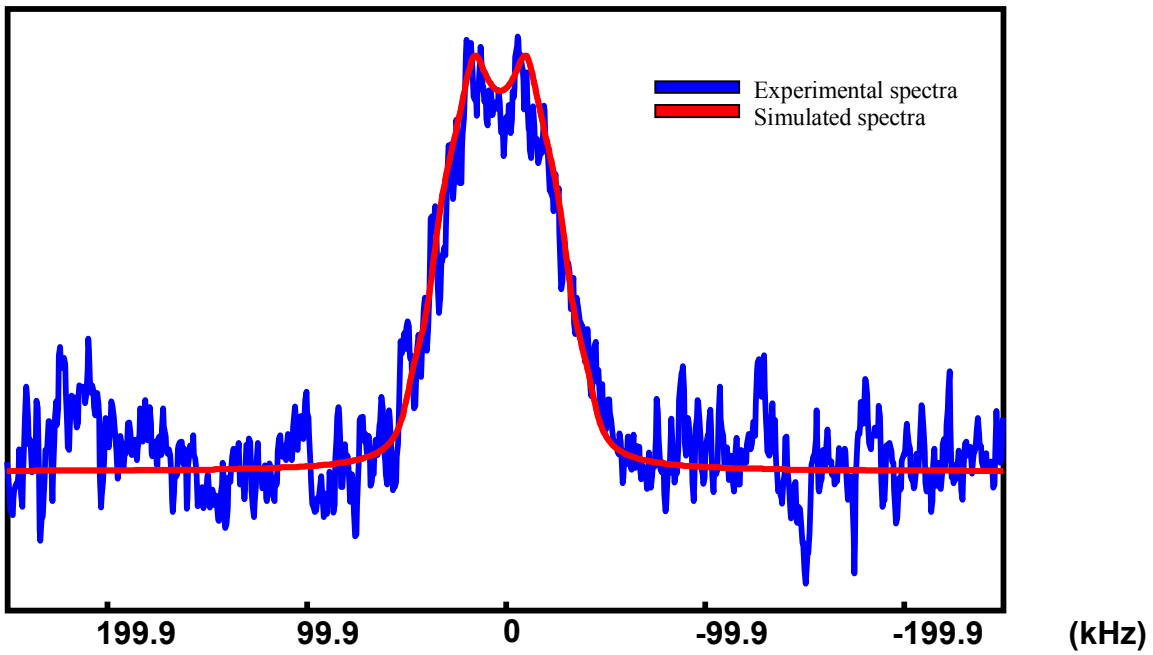

Figure 4.10: Carbon nanoflakes hydrated with D2O using a static QE experiment with d1 = 1.0 sec, d6 = 30 μsec, and d7 = μsec. This spectrum was taken in 65,546 scans with 2,048 data points.

Material	δ (kHz)	Amp	LbHz(kHz)	nuQ(kHz)	etaQ
Graphite (85%)	-3.4	1.77	11.0	110.0	0.90
Nanoflakes	2.8	15.36	9.3	92.78	0.43

Table 4.3: Summary of the simulation data taken from the carbon nanoflakes. Above this data is the data taken from the 85% D_2O hydrated graphite samples for comparision.

Chapter 5

Conclusion

In this project we have studied the hydration of carbon based materials. From the results we have determined that when placed in a constant humidity environment, sufficient water does adsorb onto the surface of graphite to perform both proton and deuteron NMR experiments. We achieved consistent results by looking at several different experiments; MAS single pulse experiments and static Quadrupole echo experiments on both graphite and carbon nanoflakes. These results are encouraging because we expect more water to both adsorb and bond to the α-CN_x films due to the presence of nitrogen making the film more reactive and providing specific binding sites. Analogous experiments need to be performed on the carbon nanotubes and α-CN_x thin films to determine if the behavior is generic to carbon based materials or specific to α-CN_x thin films.

References

1. W. J. Gammon, G. L. Hoatson, B. C. Holloway, R. L. Vold, and A. C. Reilly, *Bonding in hard and elastic amorphous carbon nitride films investigated using ^{15}N, ^{13}C, and ^{1}H NMR spectroscopy*. Phys. Rev. B **68**, 195401 (2003).
2. W. J. Gammon, D. I. Malyarenko, O. Kraft, G. L. Hoatson, A. C. Reilly, and B. C. Holloway, *Hard and elastic amorphous carbon nitride films studied by ^{13}C nuclear magnetic resonance spectroscopy*. Phys. Rev. B **66**, 153402 (2002).
3. N. J. Hinze, *Bonding and Structure*. Westminster College. http://homepages.westminster.org.uk/nick.hinze/Notes/Fifth/bondstruct.htm (2005).
4. Clark Landis, Tom Cleveland, Mary Cloninger, and David Pollock, *Buckyballs, Diamond, and Graphite*. New Traditions, Inc. www.chem.wisc.edu/~newtrad/CurrRef/BDGTopic/BDGtext/BDGGraph.html. (1996).
5. J. C. Sánchez-López and C. Donnet, *Bonding structure in amorphous carbon nitride: A spectroscopic and nuclear magnetic resonance study*. Journal of Applied Physics **90,** 975 (2001).
6. N.G. Shang, F. C. K. Au, X. M. Meng, C. S. Lee, I. Bello, and S. T. Lee, *Uniform carbon nanoflake films and their field emissions*. Chemical Physical Letters **358**, 187 (2002).

7. J. Wang, M. Zhu, X. Zhao, R. Outlaw, D. Manos, B. Holloway, C. Park, T. Anderson, and V. Mammana, *Synthesis and field-emission testing of carbon nanoflake edge emitters*. Journal of Vacuum Science & Technology B: Microelectronics and Nanometer Structures **22**, 1269 (2004).
8. V. H. Crespi, "Carbon nanostructures" Penn State University. http://www.phys.psu.edu/people/display/index.html?person_id=202;mode=research;research_description_id=419
9. J. W. Akitt, *NMR and Chemistry, an Introduction to Modern NMR Spectroscopy*, 3rd ed., (Chapman & Hall, London, 1992).
10. A. Rahman and M. Choudhary, *Solving Problems with NMR Spectroscopy*, (Academic Press, San Diego, 1996).
11. Klaus Schmidt-Rohr and Hans Wolfgang Spiess, *Multidimensional Solid-State NMR and Polymers*, (Academic Press, London, 1994).
12. Sasa Antonijevic and Stephen Wimperis, *Refocusing of chemical and paramagnetic shift anisotropies in ^2H NMR using the quadrupolar-echo experiment*, J. Mag. Res. **164**, 343 (2003).
13. D. R. Lide, *CRC Handbook of Chemistry and Physics*, 83rd ed., (CRC Press, Boca Raton, 2002).
14. K. N. Marsh, *Recommended Reference Materials for the Realization of Physiochemical Properties*, (Blackwell Scientific Publishing, Oxford, 1987).
15. D.Massiot, F.Fayon, M.Capron, I.King, S.Le Calvé, B.Alonso, J-O.Durand, B.Bujoli, Z.Gan, G.Hoatson, "Modelling one- and two-dimensional Solid State NMR spectra.", Magnetic Resonance in Chemistry **40,** 70 (2002).

16. M. Luna, J. Colchero, A. Gil, J. Gómez-Herrero, and A.M. Baró, *Application of non-contact scanning force microscopy to the study of water adsorption on graphite, gold and mica*, Applied Surface Science **157**, 393 (2000).